Computational and Structural Biotechnology Journal 24 (2024) 185–195

Contents lists available at ScienceDirect

Computational and Structural Biotechnology Journal

journal homepage: www.elsevier.com/locate/csbj

Research Article

Overcoming the cognition-reality gap in robot-to-human handovers with anisotropic variable force guidance ☆

Chaolong Qin [a], Aiguo Song [a,*], Huijun Li [a], Lifeng Zhu [a], Xiaorui Zhang [b], Jianzhi Wang [a]

[a] The State Key Laboratory of Digital Medical Engineering, Jiangsu Key Laboratory of Remote Measurement and Control, School of Instrument Science and Engineering, Southeast University, Nanjing 210096, China

[b] College of Computer and Information Engineering, Nanjing Tech University, Nanjing, 211816, China

ARTICLE INFO

Keywords:
Object handover
Home assistance
Anisotropic variable force guidance
Service robot

ABSTRACT

Object handover is a fundamental task for collaborative robots, particularly service robots. In in-home assistance scenarios, individuals often face constraints due to their posture and declining physical functions, necessitating high demands on robots for flexible real-time control and intuitive interactions. During robot-to-human handovers, individuals are limited to making perceptual judgements based on the appearance of the object and the consistent behaviour of the robot. This hinders their comprehensive perception and may lead to unexpected dangerous behaviour. Various handover trajectories pose challenges to predictive robot control and motion coordination. Many studies have shown that force guidance can provide adequate information to the receivers. However, force modulation with intention judgements based on velocity, acceleration, or jerk may impede the intended motion and require additional effort. In this paper, starting from a human-to-human handover study, an anisotropic variable force-guided robot-to-human handover control method is proposed to overcome the cognition-reality gap. The retraction motion was decoupled based on a fitted motion plane and a task-related linear trajectory, which served as a reference for overshoot suppression and impedance force modulation. The experimental results and user surveys show that the anisotropic variable impedance force suppresses overshooting without impeding the intended motions, giving the receiver sufficient time for behavioural adjustments and assisting them in completing a safe and efficient handover in a preferred manner.

1. Introduction

As people live longer and the number of patients with motor impairments caused by various diseases increases, it has become necessary to provide easier access to assisted living services and care [6]. Although many devices can be controlled remotely in compliance with ethical requirements [48–50], human-robot collaboration remains inevitable for activities of daily living (ADLs).

An object handover is a joint action between the giver and receiver, which is one of the fundamental tasks for service robots. Although handovers between humans are easy to implement [12], handovers between robots and humans face the challenges of sharing representations, predicting actions, and integrating bilateral predicted effects [42]. An effective handover requires not only the cognition of objects but also the cognition of one's abilities. Humans can be prompted by various cues for object cognition during human-to-human handovers [12,36]. However, the robot's unvarying movements and the appearance of the object impede the perception of objects, particularly for containers whose weights are closely related to their content [18,41]. Excessive force on an empty bottle or insufficient force on a full bottle can result in tipping or collision. Perceptions of one's abilities may also be biased owing to various constraints. The effort exerted to take the object must be coordinated during the handover [42].

This study focused on robot-to-human handovers in-home assistance scenarios, as shown in Fig. 1. The objective is to support individuals with motor impairments, many of whom are bedridden or rely on wheelchairs yet retain the ability to execute simple manual tasks. Manual operation constraints arise from varying body postures, physical decline, and cognitive decline [6,39], which impose more challenges

☆ This study was supported in part by the Basic Research Project of Leading Technology of Jiangsu Province under Grant No. BK20192004; in part by Jiangsu Key Research and Development Plan under Grant No.BE2023023-1; in part by National Nature Science Foundation of China under grant numbers 62272236, 62376128, 92148205; and in part by The Joint Fund Project under Grant 8091B042206.

* Corresponding author.
E-mail address: a.g.song@seu.edu.cn (A. Song).

https://doi.org/10.1016/j.csbj.2024.02.020
Received 14 December 2023; Received in revised form 26 February 2024; Accepted 26 February 2024
Available online 5 March 2024

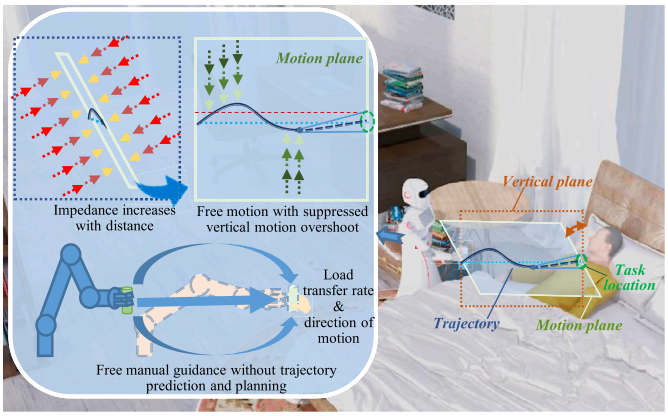

Fig. 1. Robot-to-human handovers with anisotropic variable force guidance. The robot releases objects in free, manually guided motion. To address unintentional motion overshoots without impeding intentional motions, varying impedance forces are used to suppress motions that deviate from the motion plane as well as in-plane overshoot perpendicular to the retraction direction.

in handling sensing and prediction errors, synchronising human-robot actions and adapting to user environments [3,34]. To avoid failures and improve acceptance, a handover controller must comply with the receiver instead of setting the rules [4,7]. Therefore, it is well suited for completing the handover in a compliant manually guided motion [10]. The impedance/admittance control method enables more guided and unrestricted movements than the force-free control [17], which is entirely subservient to the user, or the hybrid force-position control method, which controls the force and position separately. However, configuring the parameters requires a compromise between velocity, precision, and effort necessary for motion [28]. A promising advancement to address unintentional motion overshoots without impeding intentional motion is the use of variable impedance/admittance control. This approach provides a dynamic balance in the interactions between humans and robots [11]. However, predicting a receiver's intention based on motion characteristics alone cannot handle behaviours resulting from miscognition. The impedance force may be incorrectly reduced to account for the accelerated overshooting motion [5].

In this study, a preliminary human study was first conducted to explore the behavioural patterns the receiver preferred as their understanding of the object and manipulation skills improved. Subsequently, based on the findings and considering the primary purpose of the handover, an anisotropic variable impedance force-guided control method for a robot-to-human handover is proposed. The initial fitted motion plane of the receiver hand was used to decouple the retraction motion. The off-plane and in-plane deviations of the receiver's hand are used to anisotropically modulate the impedance force, which assists the receiver in accomplishing smooth load transfer of the object and suppressing motion overshoot without impeding the receiver's desired motion. The load transfer rate and direction of hand motion were combined for the object release judgement. Finally, an anti-overshoot capability test and robot-to-human handover feasibility test were conducted to compare the performances of the different methods. The results of these tests and a user study show that the receiver can safely and efficiently complete the desired handover using the proposed controller.

The main contributions of this work are as follows:

- Designed from the receiver's perspective, this is the first study, to our knowledge, to employ anisotropic variable-force guidance in intuitive and flexible handover motion. This approach addresses deficiencies in visual cognitive acquisition and assists receivers in coordinating unintended behaviours.
- A human-to-human handover study was conducted, leading to the development of a decoupling methodology that distinguishes between intentional and unintentional user behaviour. This methodology provides a foundation for designing controllers for effective robot-to-human handovers.
- A robot-to-human handover controller, capable of handling motion overshoot without impeding intentional motion, was designed and evaluated. This approach offers a feasible idea for assisting individuals with various manual operation constraints.

The rest of the paper is organized as follows. Section 2 provides an overview of the existing literature on robot-to-human handover study, focusing on cognition acquisition and motion accommodation. Section 3 introduces a preliminary human-to-human handover study, which served as the foundation for designing effective robot-to-human handovers. In Section 4, we outline the design of our robot-to-human handover controller. This section begins by introducing the developed controller architecture, followed by an explanation of the basic impedance control methodology. We then delve into the prediction of the plane of motion and the computation of in-plane and off-plane deviations. Finally, we propose the implementation of anisotropic variable force guidance. Section 5 presents the design of the comparative experiment and the subsequent analysis of the results. Lastly, Section 6 provides the concluding remarks for the paper.

2. Related work

Cognitive Acquisition of Receiver. Adequate cognition is fundamental to a successful handover [3,34,42]and can be used to predict the required effort in advance [18,27]. In robot-to-human handovers, the receiver's perception is primarily realized through the vision of an object's physical properties [41], the handover configuration [4], and the giver's motion [26,36,46].

When reliance is solely on visual appearance, empirical judgement may result in significant deviations in the effort required, especially for specific containers [18,27,41]. Bestick et al. considered ergonomic costs during handovers and task execution to select handover configurations. They found that the actions of the receiver could be implicitly influenced by the handover configuration for an object [8]. The giver's motion can not only indicate the initiation of a handover [30] but also enable precise positioning and softening of contact by generating human-like [25,47] and human-aware motions [45]. Learning from human demonstrations, Gaussian Mixture Models [43] and Dynamic Movement Primitives-based methods [24,38] are two other practical implementations. Moreover, Admoni et al. found that delaying the release of an object during a giver's movements captured the receiver's attention and improved compliance with gaze communication [1]. Duarte and Lastrico et al. found that the velocity of movement can indicate how carefully an object must be handled [18,27].

Cognitive Acquisition of Giver. The giver's decision regarding the object's handover location and release timing is based on an understanding of the receiver's state, capabilities, and level of control over the object.

Handover locations are influenced by many factors including different body sizes [36], arm mobility capacities [4], receiver locations, task requirements [45], kinematic features [30], and social acceptance and preferences [26]. Different ergonomic models [36] and cost functions [45] can be used depending on the scenario. To transfer objects closer, some controllers utilise gaze [33], motion, or hand-tracking systems [32,38]. The handover experience can be improved effectively through extensive data collection and model learning. However, this improvement is subject to several challenges, including prediction errors, motion synchronisation, and adaptation to the user environment.

The release timing must be coordinated because an early release may result in the fall of the object [37]. In contrast, a delayed release may result in a higher interaction force [12]. Many methods have been proposed and evaluated, including predetermined threshold [32], predetermined force-related displacement [9], load change [38], and entire load transfer [43]. Combining multiple cues has been demonstrated to be effective in releasing judgements, such as the duration of the re-

ceiver's gaze prior to touching [21] or haptic cues under sufficient load sharing [16]. However, these controllers trade-off handover smoothness with object safety [12]. Upon arriving at the pre-planned handover location, the receiver loses access to the robot's assistance and requires additional effort to release the object. A human-inspired controller [12] employs grip force modulation based on load changes, which has been proven to be effective and has been adopted by other controllers [32]. However, a greater force is required when the pulling direction changes [37].

Motion Accommodation. Learning and adapting to variable motion patterns remains a challenging task [3,11,34]. In addition to pre-assessment and prediction, real-time perception-based assistance or guidance has been proven effective [14,20]. The robot should proactively follow its human partner's movements instead of planning trajectories [5,13,14,29,47]. Variable-impedance/admittance control methods are suitable for this purpose [9,32,35]. Bazzi et al. used various impedance forces to guide a receiver's direction of motion by considering the current state of motion and a predefined target position [5]. Wu et al. considered the predictive uncertainty in impedance control with online tuning [47]. Ott et al. proposed a hybrid system approach which incorporates impedance and admittance controls [35]. Moreover, utilizing ground or aerial mobile platforms equipped with robotic arms has not only been demonstrated to capture the receiver's attention and align with their social roles and baseline proxemic preferences [23,26,46], but it has also been proven effective in adapting to complex environments and accommodating diverse human abilities and states. This approach enables ergonomic and safe physical interaction between humans and robots [2,15,44]. As for the parameter acquisition, experimental methods have often been employed to explore the parameter intervals that enable a system to be stabilised [5,19,28]. Power envelope regulation to impose constraints [14] and the automated offline generation of stable variable impedance controllers according to performance specifications [40] have been proven to be efficient. Haninger et al. addressed high-payload manual guidance with contact using admittance control [22]. Ficuciello et al. conducted an experimental study to improve the performance of human–robot physical interactions by combining Cartesian impedance modulation and redundancy resolution [19].

3. Preliminary human-to-human handover study

To establish a foundation for decoupling intended and unintended motions and exploring the appropriate release timing, a human-to-human handover study was conducted for preliminary validation.

Fig. 2 shows the experimental setup. From the receiver's perspective, they were guided to ensure their comfort during coherent retraction. This approach enables us to obtain results that tailor to individual preferences, movement constraints, and habits. Meanwhile, a giver was instructed to follow the receiver's pulling movements and release the object when deemed appropriate. To limit the the receiver's physical and cognitive functioning and immerse participants in the role, a receiver was invited to lie on a 0.75-meter-high bed and receive the object using only the thumb, index, and middle fingers of one hand. The giver delivered a glass of water weighing 580 g to the right side of the receiver's head at 45°, 0.92 m high, and 0.5 m away using only one hand [4,26,36].

36 participants (28 males and 8 females, aged between 22 and 33 years) were invited to participate in the human study. None of them had previously been involved in our system design or related research. All participants provided informed consent prior to inclusion in the study. The ethics committee of the university approved the study, and all participants provided informed consent. The participants were randomised into pairs, with one person in each group acting as the giver and the other as the receiver. The roles were exchanged for an additional five handovers after five trials. Free interviews were conducted with each experimental group.

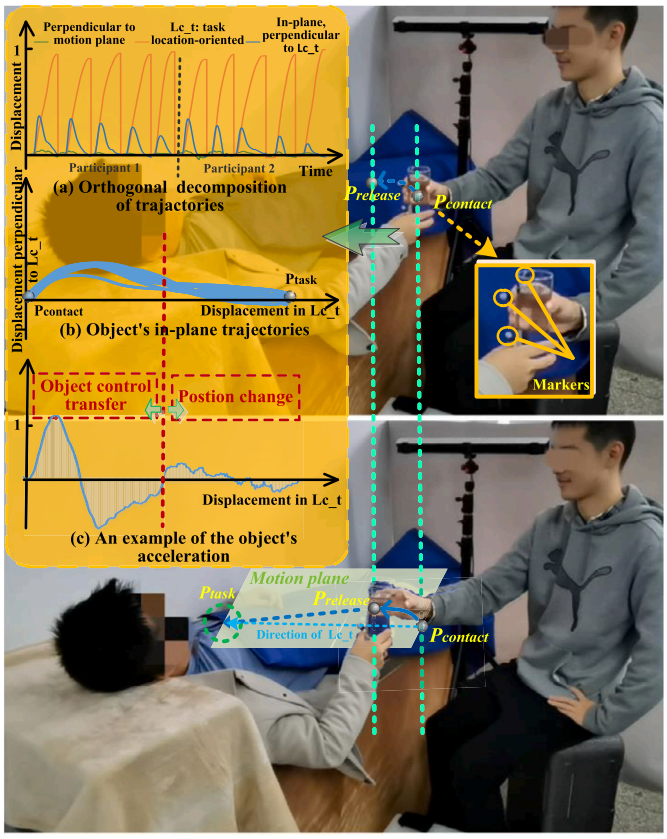

Fig. 2. A human-to-human handover scene. A receiver lies on a bed and takes a glass of water held by a giver with one hand. The giver tries to follow the receiver's guidance from the contact point $\boldsymbol{P}_{contact}$ to the release point $\boldsymbol{P}_{release}$. $\boldsymbol{Lc\_t}$ originates from $\boldsymbol{P}_{contact}$ to task location $\boldsymbol{P}_{release}$. OptiTrack markers are attached to the cup and their fingers for spatial localisation. (a) shows the orthogonal decomposition of a group's 10 handover trajectories based on a motion plane. (b) shows the object's corresponding in-plane trajectories. (c) shows a representative change in the object's acceleration.

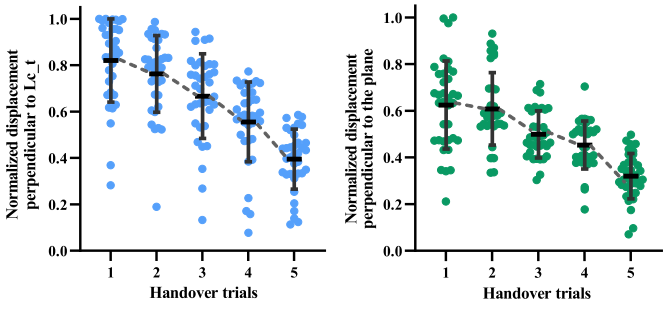

Fig. 3. The left figure illustrates the variation of maximum displacements perpendicular to $\boldsymbol{Lc\_t}$ in the plane, grouped in the order of handover. The right figure depicts the variation of maximum displacements perpendicular to the plane, also grouped in the order of handover.

Fig. 2(a-c) and Fig. 3 show the motion trajectories during the handover and the corresponding data analysis results. A plane of motion is determined based on $\boldsymbol{Lc\_t}$ and the initial direction of motion. Fig. 2(a) shows the orthogonal decomposition based on $\boldsymbol{Lc\_t}$ and the plane normal vector. The displacement in the normal vector direction of the plane was small compared to that in the other two directions. The displacements in both directions perpendicular to $\boldsymbol{Lc\_t}$ tended to increase and then decrease, with the maximum value demonstrating a tendency to decrease with the repetition of the handover. By contrast, the motion change in the direction of $\boldsymbol{Lc\_t}$ was smooth and almost unaffected by

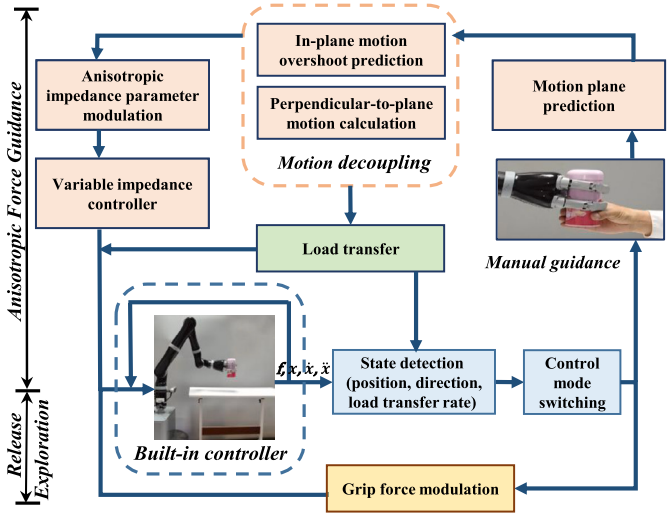

Fig. 4. System framework. Anisotropic variable force guidance involves the fusion of variable impedance forces and load forces. Release exploration is accomplished by detecting the position of the object, direction of motion, and load transfer rate.

the handover process. The trajectories shown in Fig. 2(b) and the representative acceleration changes are illustrated in Fig. 2(c) suggests that the actions of the receiver during the handover consist of two phases. The first phase involves changing the state of the object and controlling it, whereas the second phase involves transferring the object to its destination. Fig. 3 illustrates the trends of the maximum displacement in different directions.

The results of the interviews indicated that the receivers had a negative attitude towards excessive movements in both directions perpendicular to $\boldsymbol{Lc\_t}$. They described the experience as "tried [to pick it up] faster but [ended up] using excessive force", "hard to control [the force] while lying down", "easy to overshoot [to avoid falling]", "starting with too little force [and not maintaining stability]", "much better when familiar [with the situation]". The primary reasons for these movements can be summarised as a lack of understanding of the giver's release strategy, difficulty in force control in a constrained posture, and insufficient expectations of the effort required. The receivers were comforted by the givers' movements, mainly if they exerted excessive or inadequate force. In such cases, the giver's delayed release was highly appreciated, "Thank you for waiting for me to grasp it firmly". Conversely, the receivers rated it poorly, "I almost dropped it [at that time]".

Our findings are concluded as follows:

- The motion of a human receiver handover approaches a plane when it is well controlled. The receiver desires unimpeded motion towards the target location.
- A handover can be divided into object-control and position-change phases. The phase transition indicates a significant change in the receiver's level of control over the object and target of the behaviour.
- The givers' manually guided movements with unintended movement inhibition were rated highly by human receivers, particularly when mishandled or constrained.

4. Robot-to-human handover controller design

Based on the findings of the human-to-human handover study, we designed a robot-to-human handover controller using anisotropic variable-force guidance, as shown in Fig. 4. After grasp adjustment, the controller decouples the receiver's motion based on a fitted motion plane. It transfers the load and releases the object in compliant motion by utilising anisotropic variable force guidance to deal with motion overshoot. The release timing considers not only the change in motion but also the load transfer rate.

4.1. Controller architecture

The controller is divided into a pre-handover phase and a physical exchange phase. The pre-handover phase initialises the system by performing tasks including load acquisition, grip force modulation, and presenting a ready-to-handover prompt. The physical exchange phase completes the load transfer and release judgement. Fig. 4 illustrates the framework of the proposed system

In the pre-handover phase, the grip force is modulated according to the load and the maximum acceleration [37] of the handover movement using the position control [12]. Subsequently, the robot approaches the receiver from the side [4,26,36] and extends the object to the physical contact position. This action serves as a ready cue, similar to a human giver's reaching motion [30]. The physical exchange phase begins when the receiver first contacts the object and ends when the object is fully released. Load transfer and object release are performed in this process guided by anisotropic forces.

The receiver's manual guidance must be freely followed [29], impedance and admittance control are well-suited to achieve the control goal. They are complementary in stability and performance [35]. Given the force management and rapid movements involved in handovers, this study employs impedance control [19]. Note that position control is utilized during transportation to mitigate the impact of bumps and collisions. It is also employed at release to minimize motion oscillations caused by motion termination.

For safety reasons, a working area is established to prevent the object from being excessively high, low, far from, or close to the receiver. If the object breaches the working area without being released, the handover is deemed failed and will be terminated.

4.2. Fundamental Cartesian impedance control

In the study, to address the issue of undesired motions stemming from the cognition-reality gap without obstructing the desired motions of the receiver, variable impedance control [19] was utilized to facilitate anisotropic force guidance in compliant manually guided motion. Obtaining the ideal trajectory is challenging. Referring to an inaccurate motion trajectory or adding stiffness can impede the unrestricted movement of the receiver [5,14]. Therefore, no reference position or stiffness values were used in this study. The dynamic model of the robotic arm is designed as

$$\boldsymbol{M}(\boldsymbol{q})\ddot{\boldsymbol{q}} + \boldsymbol{C}(\boldsymbol{q},\dot{\boldsymbol{q}})\dot{\boldsymbol{q}} + \boldsymbol{g}(\boldsymbol{q}) + \boldsymbol{\tau}_f = \boldsymbol{\tau}_c + \boldsymbol{J}^T(\boldsymbol{q})\boldsymbol{F}_{\text{ext}} \tag{1}$$

where $\boldsymbol{M}(\boldsymbol{q})$, $\boldsymbol{C}(\boldsymbol{q},\dot{\boldsymbol{q}}) \in \mathbb{R}^{n\times n}$, $\boldsymbol{g}(\boldsymbol{q})$, $\boldsymbol{\tau}_f$, $\boldsymbol{q}$, $\dot{\boldsymbol{q}}$, $\ddot{\boldsymbol{q}} \in \mathbb{R}^n$. $\boldsymbol{M}(\boldsymbol{q})$, $\boldsymbol{C}(\boldsymbol{q},\dot{\boldsymbol{q}})$, $\boldsymbol{g}(\boldsymbol{q})$, $\boldsymbol{\tau}_f$, $\boldsymbol{\tau}_c$ are the joint space inertia, Coriolis, gravity, friction and control items of the robotic arm with n joints, respectively; $\boldsymbol{q}$, $\dot{\boldsymbol{q}}$, $\ddot{\boldsymbol{q}}$ are joint angle, angular velocity, and angular acceleration, respectively. $\boldsymbol{J}(\boldsymbol{q})$ is a Jacobian matrix. When the end-effector torque is ignored, the joint torque $\boldsymbol{\tau}_{\text{ext}} = \boldsymbol{J}^T\boldsymbol{F}_{\text{ext}}$ is generated by the external force $\boldsymbol{F}_{\text{ext}}$ on the end-effector. The end-effector was modeled as a mass–damper system, $\boldsymbol{\Lambda}_d\ddot{\boldsymbol{x}} + \boldsymbol{D}_d\dot{\boldsymbol{x}} = \boldsymbol{F}_{\text{ext}}$, where $\boldsymbol{\Lambda}_d$ and $\boldsymbol{D}_d$ are suitable diagonal inertia and damping matrices. In the Laplace domain, the one-dimensional equation can be expressed as follows:

$$V(s) = \frac{1}{D}\frac{1}{1+sT}F(s) \tag{2}$$

where V, F denote the Laplace transforms of velocity and force, respectively. $T = \lambda/D$ is the time constant of the system, where λ and D correspond to the inertia and damping along a specific Cartesian direction.

The Cartesian impedance control law can be obtained as follows.

$$\boldsymbol{\Lambda}(\boldsymbol{q})\ddot{\boldsymbol{x}} + \boldsymbol{\mu}(\boldsymbol{q},\dot{\boldsymbol{q}})\dot{\boldsymbol{x}} + \boldsymbol{F}_g(\boldsymbol{q}) + \boldsymbol{F}_f(\boldsymbol{q}) = \boldsymbol{F}_c + \boldsymbol{F}_{\text{ext}} \tag{3}$$

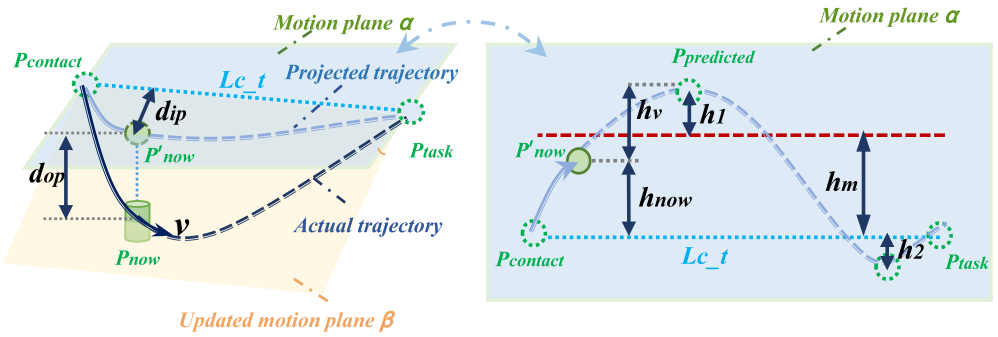

(a) Motion decoupling

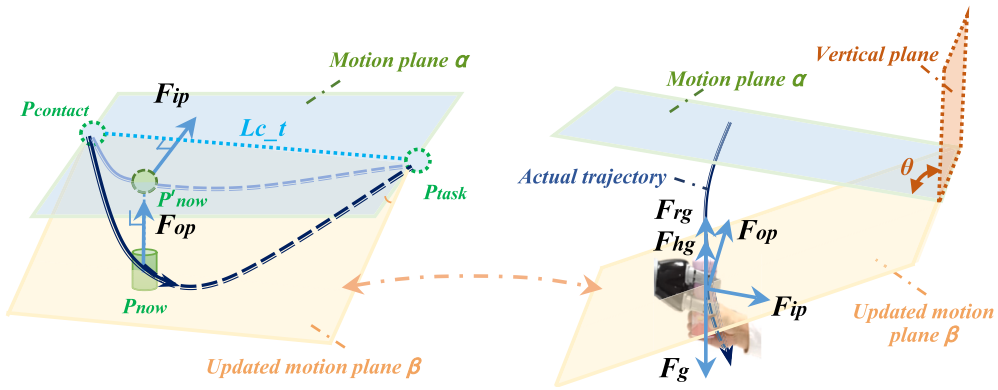

(b) Force analysis

Fig. 5. Motion decoupling and force analysis during handover. (a) illustrates the object's motion, which is decomposed into two orthogonal components: in-plane $\boldsymbol{d}_{ip}$ and off-plane $\boldsymbol{d}_{op}$, and are used to calculate the corresponding impedance forces: $\boldsymbol{F}_{ip}$ and $\boldsymbol{F}_{op}$. $\boldsymbol{h}_1$ is the positive overshoot that exceeds the predefined threshold $\boldsymbol{h}_m$, and $\boldsymbol{h}_2$ is the negative overshoot that occurs below $\boldsymbol{Lc\_t}$ connecting the contact point $\boldsymbol{P}_{contact}$ and the task point $\boldsymbol{P}_{task}$. $\boldsymbol{P}_{now'}$ is the project of $\boldsymbol{P}_{now}$ in plane α. (b) illustrates force analysis, where $\boldsymbol{F}_g$ is the object's gravitational force, $\boldsymbol{F}_{hg}$ and $\boldsymbol{F}_{rg}$ are the forces exerted by the human receiver and the robot giver, respectively. $\boldsymbol{F}_g$ is balanced by $\boldsymbol{F}_{rg}$, $\boldsymbol{F}_{hg}$ and the vertical component of $\boldsymbol{F}_{op}$ and $\boldsymbol{F}_{ip}$.

$$\boldsymbol{F}_c = \boldsymbol{\eta}(\boldsymbol{q}, \dot{\boldsymbol{q}}) - \boldsymbol{\Lambda}(\boldsymbol{q})\boldsymbol{\Lambda}_d^{-1}\boldsymbol{D}_d\dot{\boldsymbol{x}} + \left(\boldsymbol{\Lambda}(\boldsymbol{q})\boldsymbol{\Lambda}_d^{-1} - \boldsymbol{I}\right)\boldsymbol{F}_{\text{ext}} \tag{4}$$

where $\boldsymbol{x}$ denotes the Cartesian position. $\boldsymbol{\eta}(\boldsymbol{q}, \dot{\boldsymbol{q}}) = \boldsymbol{\mu}(\boldsymbol{q}, \dot{\boldsymbol{q}})\dot{\boldsymbol{x}} + \boldsymbol{F}_g(\boldsymbol{q}) + \boldsymbol{F}_f(\boldsymbol{q})$. The Cartesian parameters $\boldsymbol{\Lambda}(\boldsymbol{q})$, $\boldsymbol{\mu}(\boldsymbol{q}, \dot{\boldsymbol{q}})$, $\boldsymbol{F}_g(\boldsymbol{q})$, $\boldsymbol{F}_f(\boldsymbol{q})$, $\boldsymbol{F}_c$ are analogous items corresponding to joint space, respectively. Further details are available in [19]. The controller can effectively manipulate the end-effector in the operating space by tracking and adjusting the force applied by the operator at the end-effector while maintaining the desired impedance force based on the modulated parameters.

4.3. Motion plane prediction for motion decoupling

Based on our previous findings in Section 3, we focused on estimating the motion plane of the end-effector prior to release instead of predicting its trajectories. Fig. 5 shows the motion decoupling and force analysis during handover. The retraction along the obtained motion plane α is deemed to be in accordance with the receiver's current intention. Motion that does not overshoot within the plane α and motion towards the plane α is designed to be impervious to the impedance forces. Conversely, motion that deviates from plane α and in-plane overshoots perpendicular to the retraction direction $\boldsymbol{Lc\_t}$ is modulated by impedance forces.

Assuming that the end-effector deviates from the original motion plane α under short-term impacts, after the receiver resumes control of the handover, the receiver will pull it either to move in the updated motion plane β or back to the original plane α as Fig. 5(a) shows. Based on the initial design, any movements that minimize the deviation from α and $\boldsymbol{Lc\_t}$ would not be impeded. Moreover, updating the plane would have led to a loss of the continuous impedance force experience. Therefore, the motion plane α is maintained as a fixed reference without any updates in this study.

Due to the receiver's motion was smooth and regular after grasp adjustment, the classical total least squares method [31], which is practical and easy to implement, was used to determine the motion plane. The sum of the squares of the distances of all the data components to the plane is minimized. The handover motion serves a specific purpose: to transport the object from the giver to the task location. Therefore, to build the data source for plane fitting, 51 equidistant points were collected on the line segment $\boldsymbol{P}_{contact}\boldsymbol{P}_{task}$. Moreover, after the object had produced a 1 cm displacement, all the trajectory points were sampled at intervals greater than 2 mm within another 1 cm displacement. $\left\{\boldsymbol{P}\left(x_i, y_i, z_i\right) \mid \boldsymbol{P} \in \boldsymbol{X}_w \cap \boldsymbol{P}_l, i \in \{1, 2, \ldots, n\}\right\}$ is the sample point set. Thus, we can ascertain a motion plane that adheres to both the principles of motion and the objective of the task.

Assume that the plane equation to be found is

$$z = ax + by + c \tag{5}$$

The observed value satisfies $z_i + V_{z_i} = a\left(x_i + V_{x_i}\right) + b\left(y_i + V_{y_i}\right) + c$, where $\boldsymbol{V}_x$, $\boldsymbol{V}_y$, $\boldsymbol{V}_z$ are the corrections in the x, y, and z directions, respectively. Thus, its matrix form is

$$\left(\boldsymbol{A} + \boldsymbol{E}_A\right)\boldsymbol{X} = \boldsymbol{B} + \boldsymbol{E}_B \tag{6}$$

where $\boldsymbol{A} = \left[x_1, y_1, 1; x_2, y_2, 1; \cdots; x_n, y_n, 1\right]$, $\boldsymbol{E}_A = [V_{x_1}, V_{y_1}, 1; V_{x_2}, V_{y_2}, 1; \cdots; V_{x_n}, V_{y_n}, 1]$, $\boldsymbol{X} = [a\ b\ c]^T$, $\boldsymbol{B} = [z_1\ z_2\ \cdots\ z_n]^T$, $\boldsymbol{E}_B = [V_{z_1}\ V_{z_2}\ \cdots\ V_{z_n}]^T$. A singular value decomposition of $[\boldsymbol{A}\ \boldsymbol{B}]$ yields $\boldsymbol{C} := [\boldsymbol{A}\ \boldsymbol{B}] = \boldsymbol{U}\boldsymbol{\Sigma}\boldsymbol{V}^{\mathrm{T}}$, where $\boldsymbol{\Sigma} = \operatorname{diag}\left(\sigma_1, \ldots, \sigma_{n+d}\right)$, $\boldsymbol{U}$ are decreasing ordered singular values of $\boldsymbol{C}$, and $\boldsymbol{V} := \left[\boldsymbol{V}_{11}, \boldsymbol{V}_{12}; \boldsymbol{V}_{21}, \boldsymbol{V}_{22}\right]$.

The parameters of the plane can be obtained from the exist $\hat{\boldsymbol{X}}_{\text{tls}}$ given by

$$\hat{\boldsymbol{X}}_{\text{tls}} = -\boldsymbol{V}_{12}\boldsymbol{V}_{22}^{-1} \tag{7}$$

4.4. In-plane motion overshoot

The main factors contributing to the overshoot of the in-plane motion d_{ip} are the receiver's insufficient comprehension of the object and robot system and inadequate control of the transferred load. As illustrated in Fig. 5(a), the in-plane motion was resolved into components along $\boldsymbol{Lc\_t}$. The motion component along $\boldsymbol{Lc\_t}$ is considered as relevant to the task and should not be hindered. On the contrary, a vertical component h_1 that exceeds the set threshold h_m or a vertical component h_2 that is opposite to the initial direction is considered overshooting.

d_{ip} is given by

$$\begin{cases} d_{ip} = \begin{cases} \max\left(0, h_1\right), \text{Speed remains in the same direction} \\ h_2, \quad \text{Speed is opposite in direction} \end{cases} \\ h_1 = h_{\text{now}} + h_v - h_m \\ h_{\text{now}} = \dfrac{||\overrightarrow{\boldsymbol{P}_{\text{contact}}\boldsymbol{P}_{\text{task}}} \times \overrightarrow{\boldsymbol{P}_{\text{contact}}\boldsymbol{P}'_{\text{now}}}||}{||\overrightarrow{\boldsymbol{P}_{\text{contact}}\boldsymbol{P}_{\text{task}}}||} \end{cases} \tag{8}$$

where $\|\cdot\|$ calculates vector's Euclidean norm. $\times$ calculates vector's cross product. $\longrightarrow$ denotes the space vector formed by the two points. h_{now} is the current deviation distance. h_v is the deviation distance resulting from the deceleration of current velocity v to a complete stop in the reverse mode of the acceleration process, which is assumed to be the same as that produced when accelerating to v. h_{now} and $\dot{x}$ were recorded during the acceleration. The velocity interval that $\dot{x}$ belongs to is first determined, and then the corresponding h_v is obtained in a linearly varying manner within this interval.

Based on the feedback from the participants in the preliminary experiments, we set a criterion h_m using the height difference between $\boldsymbol{P}_{contact}$ and $\boldsymbol{P}_{task}$ as a reference, and we modulate the impedance force parameter perpendicular to the direction of $\boldsymbol{Lc\_t}$ within the motion plane α using h_1 and h_2 as references.

4.5. Off-plane deviation

A linear load transfer was performed in this study [12,37]. Typically, the closer an object is to the receiver within a specific range, the higher the perceived comfort and load acceptance capability of the receiver [4]. Therefore, instead of a fixed time, we used a predefined displacement generated by the object along $\boldsymbol{Lc\_t}$ as the basis for linear load transfer. This approach enables us to relate the load transfer to the speed at which the receiver pulls the end-effector. Specifically, a higher pulling force results in a higher speed, reflecting the greater ability of the receiver and leading to faster load transfer.

Due to load transfer or inappropriate forces applied by the receiver, the motion h_{op} that deviates from the plane α is considered undesirable. The impedance parameters in this direction are modulated accordingly. Specifically, when the object moves upward away from plane α, the portion of the vertical component of f_{op} that is not larger than the untransferred load is considered to be a transferred load and is not retaken by the robot.

Assuming $\boldsymbol{P}_{now}(x, y, z)$, according to Eq. (5), d_{op} can be obtained from the distance to the plane α.

4.6. Anisotropic variable force guidance implementation

As shown in Fig. 5(b), the impedance force is modulated according to the magnitude and direction of the d_{ip} and d_{op}, respectively. Apart from minor deviations or jittery motion of the receiver, the greater the deviation or overshoot, the more urgent it becomes to halt it. The stability regions of the parameters under realistic constraints were determined experimentally, as were the other parameters [5,19,28]. Thus, the damping D is heuristically modulated as follows:

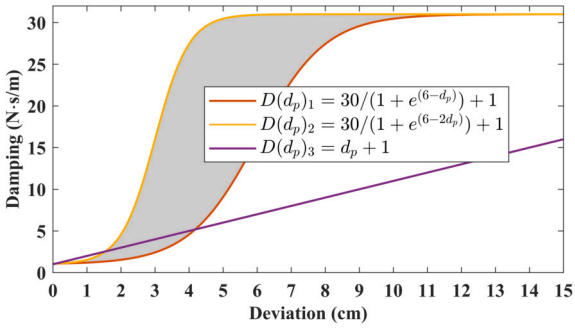

Fig. 6. Damping values versus the deviation values. $D(d_p)_1$ and $D(d_p)_2$ represent δ sets 90° and 0°, respectively. $D(d_p)_3$ shows equivalent variation curves of damping versus deviation for comparison. The shaded area is the range of possible distributions of the damping change curve due to the change in angle between the motion plane and the vertical plane.

$$D(d_p) = 30/(1+e^{(6-\delta d_p)})+1, d_p \in \{d_{ip}, d_{op}\} \tag{9}$$

where as Fig. 5 shows, δ reflects the ease of deviation from plane α and is taken as $(1+cos\theta)$. θ represents the angle between plane α and vertical direction.

Fig. 6 shows the correspondence between the damping and deviation values. λ is set with a constant low value of 1.5 kg, which is close to the minimum value within the stability region [19]. When no overshooting occurs, the impedance force is maintained at its minimum value, which ensures system stability. However, when the deviation d_p increases, the damping D increases and the inertia λ decreases rapidly, enabling the receiver to suppress the overshoot quickly. It is noteworthy that the accurate measurement of the parameter stabilisation intervals in each direction is almost impossible and unnecessary. To ensure system stability, the strictest stabilisation interval in the vertical direction was selected as a conservative solution.

Consideration must be given to the time required to release an object during force guidance. The release of an object requires the receiver to control the object completely. According to our previous findings in Section 3, the transition from the object control transfer phase to the position change phase can be considered appropriate timing. Alterations in the direction of motion are crucial indicators of this change. Fig. 7 and Eq. (10) depict the situation at release, where the distance d_v in which the direction of $\dot{\boldsymbol{x}}$ deviates from $\boldsymbol{P}_{task}$ and the load transfer rate $r_{transfer}$ are utilized as release cues:

$$\begin{cases} \text{ReleaseSignal} = \left(d_v < d\right) \wedge \left(r_{\text{transfer}} > \varepsilon\right) \\ d_v = \dfrac{||\overrightarrow{\boldsymbol{P}_{\text{now}}\boldsymbol{P}_{\text{task}}} \times \dot{\boldsymbol{x}}||}{||\dot{\boldsymbol{x}}||} \end{cases} \tag{10}$$

where $\|\cdot\|$ calculates vector's Euclidean norm. $\times$ calculates vector's cross product. $\longrightarrow$ denotes the space vector formed by the two points. d is a pre-determined threshold for d_v, ε is a pre-determined threshold for r_{transfer}.

Algorithm 1 demonstrates a complete handover process with anisotropic variable force guidance.

5. Experiments

This section first evaluates the capability of an anisotropic variable impedance controller (AVI) to handle in-plane and off-plane overshoots under plane-invariant conditions. Handover performance was subsequently assessed using a feasibility test. The former test was compared with a constant-low-impedance controller (CLI), constant-medium-impedance controller (CMI), and constant-high-impedance controller (CHI). The latter test was compared with CLI and a proven effective

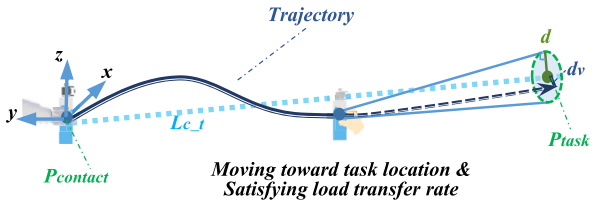

Fig. 7. Release detection. The object is released when it is moving towards the task location $\boldsymbol{P}_{task}$ and the load transfer condition is met. A small tolerance d is introduced to account for the computational error and the human motion uncertainty.

Algorithm 1: Anisotropic Variable Force-guided Handover Controller.

Input: End-effector position: $\boldsymbol{x}$, Cartesian force: $\boldsymbol{F}_{pull}$, Physical contact: $\boldsymbol{P}_{contact}$, Task location: $\boldsymbol{P}_{task}$, Initial Cartesian force: $\boldsymbol{F}_{init}$
Output: releaseSignal, releaseResult

linePointSet $\boldsymbol{P}_n$ = sampleLine($\boldsymbol{P}_{contact}$, $\boldsymbol{P}_{task}$);
load $\boldsymbol{F}_{load}$ = getLoad($\boldsymbol{F}_{init}$);
while *inWorkingArea and objectUnreleased* **do**
  $\dot{\boldsymbol{x}}$, $\ddot{\boldsymbol{x}}$ = getVelocityAndAcceleration ($\boldsymbol{x}$);
  $\boldsymbol{X}$,$\dot{\boldsymbol{X}}$,$\ddot{\boldsymbol{X}}$ = recordTrajVelAcc($\boldsymbol{x}$, $\dot{\boldsymbol{x}}$, $\ddot{\boldsymbol{x}}$);
  $\boldsymbol{X}_w$ = sampleSlidingWindowInTrajectory($\boldsymbol{X}$);
  objectGrasped = $\boldsymbol{F}_{pull}$ > thresholdToCoverNoise;
  if *objectGrasped* **then**
    compensateGravitywithMiniImpedance($\boldsymbol{F}_{load}$);
  end
  if *not planeObtained* **then**
    Plane α = getByTotalLeastSquares($\boldsymbol{X}_w$,$\boldsymbol{P}_n$);
  else
    d_{ip}, d_{op} = getDeviation($\boldsymbol{x}$, $\dot{\boldsymbol{x}}$, $\boldsymbol{X}$, $\dot{\boldsymbol{X}}$, α, $\boldsymbol{P}_{contact}$, $\boldsymbol{P}_{task}$);
    $\boldsymbol{F}_{ip}$,$\boldsymbol{F}_{op}$ = getImpedanceForces($\dot{\boldsymbol{x}}$,$\ddot{\boldsymbol{x}}$,d_{ip},d_{op});
    $\boldsymbol{F}_{load}$ = transferLoad($\boldsymbol{x}$, $\boldsymbol{F}_{load}$);
    outputCombinedForce, $r_{transfer}$ = ($\boldsymbol{F}_{ip}$, $\boldsymbol{F}_{op}$, $\boldsymbol{F}_{load}$);
    d_v = getVelocityDirectionDeviation($\boldsymbol{x}$,$\dot{\boldsymbol{x}}$,$\boldsymbol{P}_{task}$);
  end
  releaseSignal,releaseResult = checkDirectionAndTransferRate($\boldsymbol{x}$,d_v,$r_{transfer}$);
end

human-inspired handover controller (HI). The CMI, CHI, and controllers employing trajectory planning strategies were not chosen because of their significant hindering effect on the receiver's free retraction motion, which did not fit the handover task in our setup scenario.

The average velocity was calculated as the instantaneous velocity using the positions within a sliding window of 0.03 s. The instantaneous acceleration was similarly obtained using the velocity. The resulting force values were pre-processed using a 4th-order Butterworth low-pass filter with a cutoff frequency of 5 Hz. The critical values must be confirmed after several consecutive confirmations to cover the jitter. For instance, confirmation of the velocity direction requires three consecutive frames to satisfy the release condition.

5.1. System setup

As illustrated in Fig. 8, our experiments were conducted on a mobile platform that was equipped with a 6.18 kg 7-degree-of-freedom Kinova JACO2 lightweight robotic arm featuring a three-finger gripper. Each joint of the robotic arm was equipped with a torque sensor. An Intel RealSense D455 RGB-D camera was used for recognition and localisation. The system was implemented at 100 Hz within the framework of the Robot Operating System (ROS) framework. An OptiTrack V120 Trio motion-tracking system was used for evaluation.

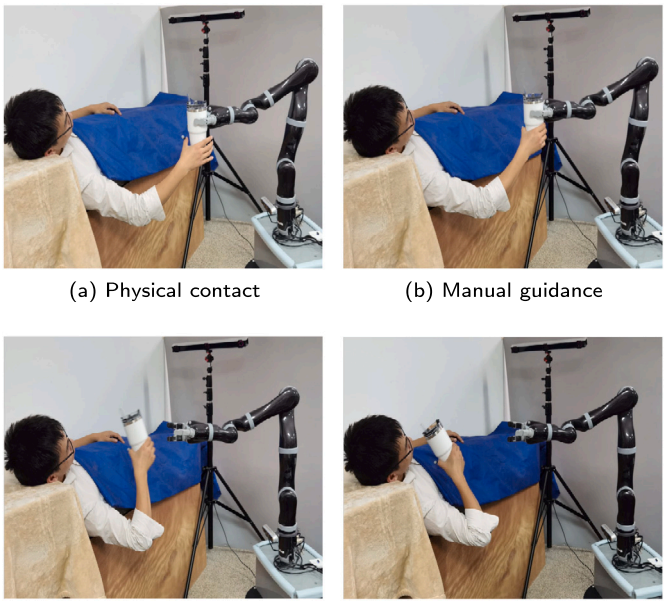

Fig. 8. An example of robot-to-human handover, where a receiver completes the handover in a prone position.

5.2. Anti-overshoot capability test

To evaluate the effect of anisotropic variable-force guidance on mitigating overshoot motion, we conducted quantitative overshoot simulation experiments. The motion plane was assumed to be a constant vertical plane. Since it is almost impossible to generate reproducible overshoot using human traction, we provided an end-effector force control signal that linearly decreased from 10 N to 0 N for 0.5 seconds to simulate the generation of overshoot. A force signal is applied horizontally. The suppression capability in the other directions was similar to that in the vertical direction. The difference lies in the use of a load force for overshoot suppression in the vertical direction, which enables an efficient load transfer. A detailed explanation is provided in Section 4.5.

The AVI parameters are described in Section 4.6. CLI, CMI, and CHI use minimum damping, half damping, and maximum damping, respectively, in the range set to maintain system stability. The inertial parameters were kept consistent across the controllers. Each of the four controllers was used to perform the test 10 times.

Table 1 and Fig. 9 shows their anti-overshoot performance. Under the same force application conditions, the overshoot produced by CHI is the lowest, while CLI produces the highest overshoot. AVI(0°) produces an overshoot between CMI and CHI, and AVI(90°) produces an overshoot between CMI and CLI. Settling time is defined as the time required to reach the maximum overshoot. The results are consistent with those described above. At the onset time, Both AVI's displacement change is similar to CLI's, indicating less obstruction. As the deviation increases, AVI(0°)'s performance comes closer to CMI, and AVI(90°)'s performance comes closer to CHI.

5.3. Feasibility test

A robot-to-human handover study was conducted to validate the practical performance of the proposed controller for handover tasks. Fig. 8 shows an example of the experimental scenario.

To ensure that the area of perceived safety was not violated, the entire load was transferred at half of the overall displacement. Specifically, the load transfer speed in the Lc-t direction was 0.26 N/cm. ε and d in Eq. (10) were set as 60% and 10 cm, respectively.

Table 1
Anti-overshoot Performance of the Proposed Anisotropic Variable Impedance Controller Versus Different Constant Impedance Controllers.

Controller	AVI(0°)	AVI(90°)	CLI	CMI	CHI
Displacement (m)	0.09 ± 0.01	0.12 ± 0.02	0.17 ± 0.05	0.10 ± 0.01	0.07 ± 0.01
Settling time (s)	0.53 ± 0.04	0.58 ± 0.04	1.30 ± 0.17	0.58 ± 0.01	0.51 ± 0.01

means ± standard deviation

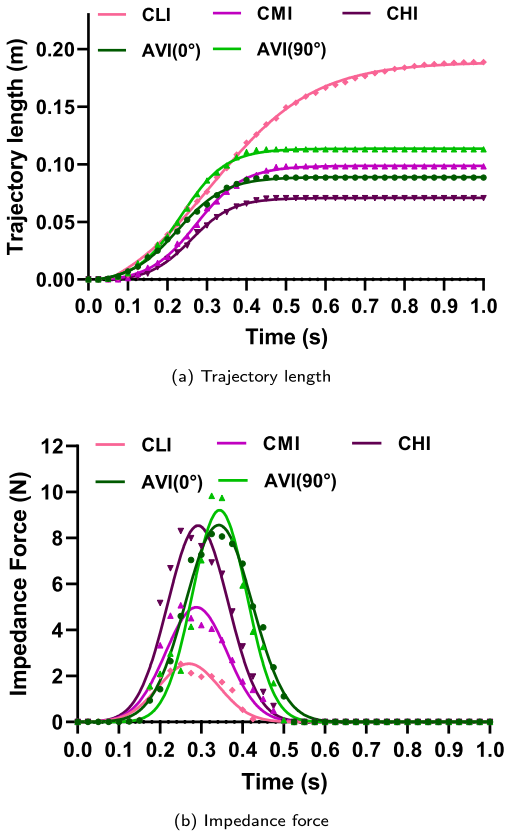

(a) Trajectory length

(b) Impedance force

Fig. 9. The performance of different controllers in the direction of the force under the same force pattern. (a) illustrates the resulting trajectory length, which represents the magnitude of motion overshoot. (b) depicts the generated impedance force. For simplicity, only a portion of the sample points is shown.

Table 2
Performance of Different Controllers in the Feasibility Test.

Controller	Task completion time (s)	Maximum overshoot (m)	Trajectory length (m)	Receiver effort (J)
AVI	1.88 ± 0.15	**0.11 ± 0.02**	**0.52 ± 0.01**	**1.32 ± 0.25**
CLI	1.92 ± 0.25	0.14 ± 0.02	0.55 ± 0.02	1.85 ± 0.32
HI	1.79 ± 0.57	0.15 ± 0.04	0.56 ± 0.02	2.31 ± 0.49

means ± standard deviation

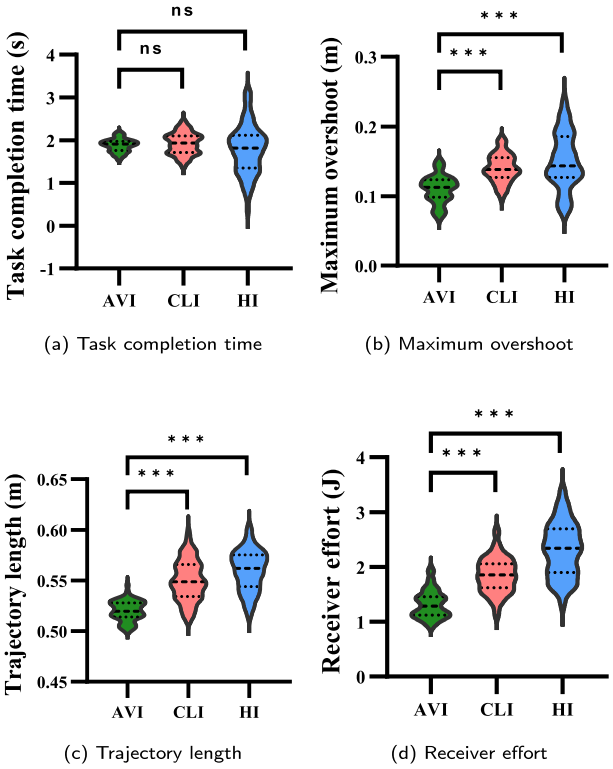

(a) Task completion time

(b) Maximum overshoot

(c) Trajectory length

(d) Receiver effort

Fig. 10. Performance of each controller.

22 participants (18 males and four females, aged 23–56 years) were invited to participate in our study. None of the authors had previously been involved in our system design or related research. All participants provided informed consent prior to inclusion in the study. The ethics committee of the university approved the study, and all participants provided informed consent.

Each participant participated individually in the experiment. To familiarise the participants with the task requirements, each controller was experienced twice prior to the experiment. The following experiment employed a setup similar to that described in Section 3, where participants were asked to comfortably pick up a cup from a fixed location and bring it to another fixed location for drinking.

Considering that the mass of the objects manipulated in the home assistance scenario would not be too heavy, we used three opaque metal cups of the same appearance filled with different weights of water: 333 g, 667 g, and 1,000 g. This setting is intended to create a gap between the receiver's cognition and reality. Each cup was delivered using AVI, CLI, and HI for 9 trials, with the order of execution randomised to eliminate order effects as much as possible. The three trials completed by each participant using the same controller were treated as a group to eradicate the influence of mass on the evaluation results.

At the end of each trial, each participant was invited to participate in a survey. Interviews were conducted at the end of the experiments. The survey was designed as follows:

1. Rate how easy it was to take an object for each handover (1 = very hard to take, 5 = very easy to take).
2. Rate the preference level for each handover (1 = not at all preferred, 5 = highly preferred)

Table 2 and Fig. 10 illustrate the performance of different controllers in the feasibility test. The metrics chosen for evaluation include *Task completion time*, *Maximum overshoot*, *Trajectory length*, and *Receiver effort*. Ease of control and adaptation to preferences were as-

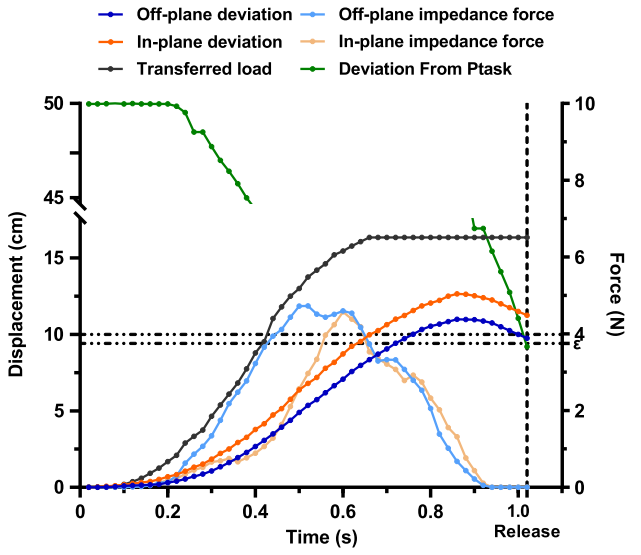

Fig. 11. Changes in the in-plane and off-plane deviations, the corresponding impedance forces, and the load transfer for a representative handover.

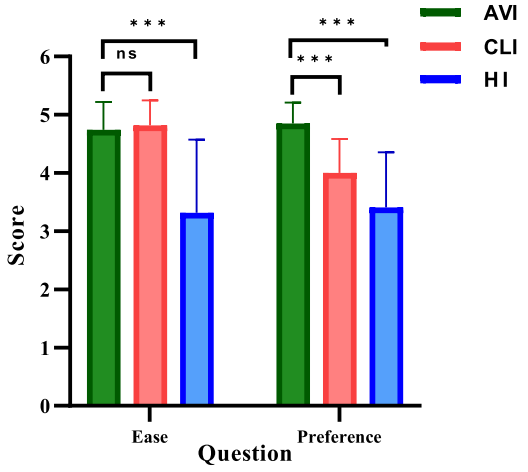

Fig. 12. Mean and variance of participants' perception of ease and preference.

sessed through surveys and free interviews. Each trial begins with a physical contact moment and ends with the moment when the object completes a fixed displacement. *Task completion time* is the time required for a total trial. *Maximum overshoot* is the displacement from line $\boldsymbol{L}c\_t$. *Trajectory length* calculates the object's trajectory length during one trial. *Receiver effort* is calculated as the cumulative change in the sum of the object's kinetic and potential energies minus the work done by the impedance force.

Fig. 11 illustrates the synchronisation of the impedance force with the corresponding in-plane and off-plane deviations during handover. Additionally, the variation in the load force and deviation is illustrated in the direction of the velocity used for the release judgement during the process. As not all data passed both the Shapiro-Wilk normality test and Mauchly's test of sphericity, they were analysed using the non-parametric Friedman test with Dunn-Bonferroni post hoc instead of a one-way repeated-measures analysis of variance (ANOVA) test. The Friedman test result showed no significant difference in *Task completion time* ($\chi^2(2) = 3.364, p = 0.186 > 0.05$). However, there were significant differences in *Maximum overshoot* ($\chi^2(2) = 49.182, p < 0.001$), *Trajectory length* ($\chi^2(2) = 82.394, p < 0.001$) and *Receiver effort* ($\chi^2(2) = 79.121, p < 0.001$). Compared to CLI and HI, AVI exhibited a significantly lower maximum overshoot ($p < 0.001$), shorter trajectory length ($p < 0.001$), and less receiver effort ($p < 0.001$).

Fig. 12 shows the survey results. The Friedman test results ($\chi^2(2) = 86.311, p < 0.001$) indicated that it was significantly easier to take objects using AVI than HI ($p < 0.001$). However, there was no significant difference between AVI and CLI in this aspect ($p > 0.05$). Meanwhile, AVI was significantly more preferred than CLI ($p < 0.001$) and HI ($p < 0.001$) ($\chi^2(2) = 87.559, p < 0.001$).

In the interviews, the participants reported that owing to postural constraints and a change in the way they generated force in their upper extremities, their manual operation ability was significantly reduced from their routine when lying down. Moreover, the uniform appearance of the cup creates uncertainty regarding the amount of force that should be applied while handling the cup. These challenges lead to undesirable movements while picking up objects. The anisotropic variable-force-guided controller was found to quickly pick up the object and suppress the overshoot, thereby helping them accomplish the change in force generation required to take over the object. The movements with the constant-low-impedance controller were smooth but had little suppression of overshoot and could not be stopped quickly. In contrast, for HI, they could take the object efficiently only when they were aware of the setting rules.

5.4. Discussion & limitation

According to the experimental results, AVI performs better with regard to maximum overshoot, trajectory length, and receiver effort but does not stand out in task completion time. One possible reason for this is that the task completion time is relevant not only to the controller's efficiency but also to the receiver's mindset. During the experiment, we observed that the participants tended to move more slowly when they felt safe and comfortable. Conversely, during accidents, they tend to move much faster to mitigate the risk of falling. This phenomenon has a significant impact on the task completion time. AVI and CVI performed comparably in terms of ease, indicating that neither system hindered the desired handover behaviour. However, AVI was preferred over CVI, suggesting that the anisotropic impedance force played a positive role.

In our study, we employed a predetermined rule for the alteration of the impedance parameters and selected the angle between the fitted plane of motion and the vertical plane to regulate their changes. However, it is worth investigating how to personalise the speed of the impedance change to cater to the varying desired effects among different groups of individuals.

Anisotropic variable-force guidance is employed to address the issue of overshooting that may occur owing to the cognitive-reality gap or load transfer when performing handovers. The experimental results demonstrated that our intervention was effective. However, additional user studies and onsite utilisation tests must be conducted to refine the user behaviour model and improve the adaptability of the controller. Further investigations into the causes of overshoot, such as enhancing the receiver's perception of the object or investigating in-depth load-transfer strategies, could be beneficial for avoiding or mitigating motion overshoot. Moreover, dynamically modulating grip force according to the motion state is a promising direction for improvement.

6. Conclusion

In this study, we introduce a decoupling methodology that distinguishes between intentional and unintentional user behaviour, andpropose an anisotropic variable force-guided handover control method for individuals facing various manual operation constraints inhome assistance scenarios. The robot-to-human handovers are facilitated by considering the preferred behavioural patterns obtained from a human handover study. Displacements that deviated from the fitted motion plane and the fundamental task-related movement were used to modulate the impedance force. This modulation enables the receiver to consistently

receives ongoing support from the robot and freely pull the object to a suitable location with minimal effort. The anisotropic variable force addresses unintentional motion overshoots without impeding intentional motions based on the purpose of the handover, assisting in the smooth transfer of loads and improving the safety of the handover. Comparative experiments with different controllers and user surveys showed that the proposed controller enables a safe, efficient, and easily controlled handover.

CRediT authorship contribution statement

Conceptualization: Chaolong Qin, Aiguo Song; Methodology: Chaolong Qin, Aiguo Song; Formal analysis and investigation: Chaolong Qin, Huijun Li, Lifeng Zhu, Jianzhi Wang; Writing - original draft: Chaolong Qin; Writing - review and editing: Chaolong Qin, Aiguo Song, Huijun Li, Lifeng Zhu, Xiaorui Zhang, Jianzhi Wang; Funding acquisition: Aiguo Song, Xiaorui Zhang; Resources: Aiguo Song; Supervision: Aiguo Song, Chaolong Qin. All authors read and approved the final manuscript.

Declaration of competing interest

The authors declare that they have no known competing financial interests or personal relationships that could have appeared to influence the work reported in this paper.

References

[1] Admoni H, Dragan A, Srinivasa SS, Scassellati B. Deliberate delays during robot-to-human handovers improve compliance with gaze communication. In: Proc. ACM/IEEE int. conf. hum.–robot interact.; 2014. p. 49–56.

[2] Afifi A, van Holland M, Franchi A. Toward physical human-robot interaction control with aerial manipulators: compliance, redundancy resolution, and input limits. In: Proc. IEEE int. conf. robot. automat. IEEE; 2022. p. 4855–61.

[3] Ajoudani A, Zanchettin AM, Ivaldi S, Albu-Schäffer A, Kosuge K, Khatib O. Progress and prospects of the human–robot collaboration. Auton Robots 2018;42:957–75.

[4] Ardón P, Cabrera ME, Pairet E, Petrick RP, Ramamoorthy S, Lohan KS, et al. Affordance-aware handovers with human arm mobility constraints. IEEE Robot Autom Lett 2021;6:3136–43.

[5] Bazzi D, Lapertosa M, Zanchettin AM, Rocco P. Goal-driven variable admittance control for robot manual guidance. In: Proc. IEEE/RSJ int. conf. intell. robots syst.; 2020. p. 9759–66.

[6] Beard JR, Officer A, De Carvalho IA, Sadana R, Pot AM, Michel JP, et al. The world report on ageing and health: a policy framework for healthy ageing. Lancet 2016;387:2145–54.

[7] Bedaf S, Draper H, Gelderblom GJ, Sorell T, de Witte L. Can a service robot which supports independent living of older people disobey a command? The views of older people, informal carers and professional caregivers on the acceptability of robots. Int J Soc Robot 2016;8:409–20.

[8] Bestick A, Bajcsy R, Dragan AD. Implicitly assisting humans to choose good grasps in robot to human handovers. In: Proc. int. symp. exp. robot. Springer; 2016. p. 341–54.

[9] Bohren J, Rusu RB, Jones EG, Marder-Eppstein E, Pantofaru C, Wise M, et al. Towards autonomous robotic butlers: lessons learned with the pr2. In: Proc. IEEE int. conf. robot. automat.; 2011. p. 5568–75.

[10] Calanca A, Muradore R, Fiorini P. A review of algorithms for compliant control of stiff and fixed-compliance robots. IEEE/ASME Trans Mechatron 2015;21:613–24.

[11] Calanca A, Muradore R, Fiorini P. A review of algorithms for compliant control of stiff and fixed-compliance robots. IEEE/ASME Trans Mechatron 2015;21:613–24.

[12] Chan WP, Parker CA, Van der Loos HM, Croft EA. A human-inspired object handover controller. Int J Robot Res 2013;32:971–83.

[13] Chan WP, Tran T, Sheikholeslami S, Croft E. An experimental validation and comparison of reaching motion models for unconstrained handovers: towards generating humanlike motions for human-robot handovers. In: Proc. IEEE-RAS int. conf. humanoid robots. IEEE; 2021. p. 356–61.

[14] Chen J, Ro PI. Human intention-oriented variable admittance control with power envelope regulation in physical human-robot interaction. Mechatronics 2022;84:102802.

[15] Corsini G, Jacquet M, Das H, Afifi A, Sidobre D, Franchi A. Nonlinear model predictive control for human-robot handover with application to the aerial case. In: Proc. IEEE/RSJ int. conf. intell. robots syst. IEEE; 2022. p. 7597–604.

[16] Costanzo M, De Maria G, Natale C. Handover control for human-robot and robot-robot collaboration. Front Robot AI 2021;8:672995.

[17] Dong K, Liu H, Zhu X, Wang X, Xu F, Liang B. Force-free control for the flexible-joint robot in human-robot interaction. Comput Electr Eng 2019;73:9–22.

[18] Duarte NF, Chatzilygeroudis K, Santos-Victor J, Billard A. From human action understanding to robot action execution: how the physical properties of handled objects modulate non-verbal cues. In: Proc. IEEE int. conf. dev. learn. epigenetic robot.; 2020. p. 1–6.

[19] Ficuciello F, Villani L, Siciliano B. Variable impedance control of redundant manipulators for intuitive human–robot physical interaction. IEEE Trans Robot 2015;31:850–63.

[20] Gienger M, Ruiken D, Bates T, Regaieg M, MeiBner M, Kober J, et al. Human-robot cooperative object manipulation with contact changes. In: Proc. IEEE/RSJ int. conf. intell. robots syst. IEEE; 2018. p. 1354–60.

[21] Grigore EC, Eder K, Pipe AG, Melhuish C, Leonards U. Joint action understanding improves robot-to-human object handover. In: Proc. IEEE/RSJ int. conf. intell. robots syst.; 2013. p. 4622–9.

[22] Haninger K, Radke M, Vick A, Krüger J. Towards high-payload admittance control for manual guidance with environmental contact. IEEE Robot Autom Lett 2022;7:4275–82.

[23] He K, Simini P, Chan WP, Kulić D, Croft E, Cosgun A. On-the-go robot-to-human handovers with a mobile manipulator. In: Proc. 31st int. conf. robot human interact. commun. IEEE; 2022. p. 729–34.

[24] Iori F, Perovic G, Cini F, Mazzeo A, Falotico E, Controzzi M. Dmp-based reactive robot-to-human handover in perturbed scenarios. Int J Soc Robot 2023;15:233–48.

[25] Kajikawa S, Okino T, Ohba K, Inooka H. Motion planning for hand-over between human and robot. In: Proc. IEEE/RSJ int. conf. intell. robots syst./hum. robot interact. cooperative robots; 1995. p. 193–9.

[26] Koay KL, Syrdal DS, Ashgari-Oskoei M, Walters ML, Dautenhahn K. Social roles and baseline proxemic preferences for a domestic service robot. Int J Soc Robot 2014;6:469–88.

[27] Lastrico L, Garello L, Rea F, Noceti N, Mastrogiovanni F, Sciutti A, et al. Robots with different embodiments can express and influence carefulness in object manipulation. In: Proc. IEEE int. conf. dev. learn. IEEE; 2022. p. 280–6.

[28] Lecours A, Mayer-St-Onge B, Gosselin C. Variable admittance control of a four-degree-of-freedom intelligent assist device. In: Proc. IEEE int. conf. robot. automat.; 2012. p. 3903–8.

[29] Li Y, Yang L, Huang D, Yang C, Xia J. A proactive controller for human-driven robots based on force/motion observer mechanisms. IEEE Trans Syst Man Cybern Syst 2022.

[30] Liu D, Wang X, Cong M, Du Y, Zou Q, Zhang X. Object transfer point predicting based on human comfort model for human-robot handover. IEEE Trans Instrum Meas 2021;70:1–11.

[31] Markovsky I, Van Huffel S. Overview of total least-squares methods. Signal Process 2007;87:2283–302.

[32] Medina JR, Duvallet F, Karnam M, Billard A. A human-inspired controller for fluid human-robot handovers. In: Proc. IEEE-RAS int. conf. humanoid robots; 2016. p. 324–31.

[33] Moon A, Troniak DM, Gleeson B, Pan MK, Zheng M, Blumer BA, et al. Meet me where I'm gazing: how shared attention gaze affects human-robot handover timing. In: Proc. ACM/IEEE int. conf. hum.–robot interact.; 2014. p. 334–41.

[34] Ortenzi V, Cosgun A, Pardi T, Chan WP, Croft E, Kulić D. Object handovers: a review for robotics. IEEE Trans Robot 2021;37:1855–73.

[35] Ott C, Mukherjee R, Nakamura Y. Unified impedance and admittance control. In: Proc. IEEE int. conf. robot. automat.; 2010. p. 554–61.

[36] Parastegari S, Abbasi B, Noohi E, Zefran M. Modeling human reaching phase in human-human object handover with application in robot-human handover. In: Proc. IEEE/RSJ int. conf. intell. robots syst.; 2017. p. 3597–602.

[37] Parastegari S, Noohi E, Abbasi B, Žefran M. Failure recovery in robot–human object handover. IEEE Trans Robot 2018;34:660–73.

[38] Prada M, Remazeilles A, Koene A, Endo S. Implementation and experimental validation of dynamic movement primitives for object handover. In: Proc. IEEE/RSJ int. conf. intell. robots syst.; 2014. p. 2146–53.

[39] Qin C, Song A, Wei L, Zhao Y. A multimodal domestic service robot interaction system for people with declined abilities to express themselves. Intell Serv Robot 2023:1–20.

[40] San-Miguel A, Alenyà G, Puig V. Automated off-line generation of stable variable impedance controllers according to performance specifications. IEEE Robot Autom Lett 2022;7:5874–81.

[41] Sanchez-Matilla R, Chatzilygeroudis K, Modas A, Duarte NF, Xompero A, Frossard P, et al. Benchmark for human-to-robot handovers of unseen containers with unknown filling. IEEE Robot Autom Lett 2020;5:1642–9.

[42] Sebanz N, Knoblich G. Prediction in joint action: what, when, and where. Top Cogn Sci 2009;1:353–67.

[43] Sidiropoulos A, Psomopoulou E, Doulgeri Z. A human inspired handover policy using Gaussian mixture models and haptic cues. Auton Robots 2019;43:1327–42.

[44] Silano G, Afifi A, Saska M, Franchi A. A signal temporal logic planner for ergonomic human–robot collaboration. In: Proc. int. conf. on unmanned aircraft systems. IEEE; 2023. p. 328–35.

[45] Sisbot EA, Alami R. A human-aware manipulation planner. IEEE Trans Robot 2012;28:1045–57.

[46] Wojciechowska A, Frey J, Sass S, Shafir R, Cauchard JR. Collocated human-drone interaction: methodology and approach strategy. In: Proc. 14th ACM/IEEE int. conf. hum.–robot interact. IEEE; 2019. p. 172–81.

[47] Wu M, Taetz B, Saraiva ED, Bleser G, Liu S. On-line motion prediction and adaptive control in human-robot handover tasks. In: Proc. IEEE int. conf. adv. robot. social impacts. IEEE; 2019. p. 1–6.
[48] Xu B, Liu D, Xue M, Miao M, Hu C, Song A. Continuous shared control of a mobile robot with brain–computer interface and autonomous navigation for daily assistance. Comput Struct Biotechnol J 2023;22:3–16.
[49] Zhang X, Sun X, Sun X, Sun W, Jha SK. Robust reversible audio watermarking scheme for telemedicine and privacy protection. Comput Mater Continua 2022;71:3035–50.
[50] Zhang X, Zhang W, Sun W, Sun X, Jha SK. A robust 3-d medical watermarking based on wavelet transform for data protection. Comput Syst Sci Eng 2022;41:1043–56.